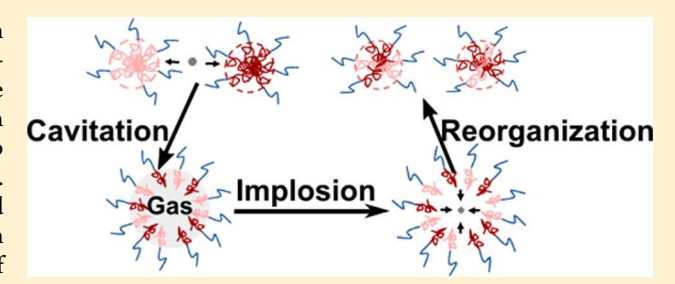
Nacromolecules 2018, 51, 6967–6975

Cavitation Enables Switchable and Rapid Block Polymer Exchange under High-xN Conditions

Kayla A. Lantz, † Amrita Sarkar, †,# Kenneth C. Littrell, † Tianyu Li, \$,|| Kunlun Hong, \$,|| © and Morgan Stefik*,†®

Supporting Information

ABSTRACT: Kinetically trapped micelles are a novel platform for diverse emerging applications. However, their homogenization and reproducibility is inherently challenging due to the high-\(\gamma N \) barrier toward chain exchange processes. Sonication enables switchable micelle exchange where cavitation leads to exchange and cessation returns micelles to kinetic entrapment. The mechanism was posited to be an agitation induced exchange process similar to recent developments with vortexing. This study reports the first SANS measurements of chain exchange during cavitation induced exchange (CIE). The



mixed chain concentration progresses linearly with sonication time, analogous to vortexing. In contrast, the rate of CIE was directly proportional to the polymer concentration. This feature indicates that CIE uniquely overcomes the energetic barriers that reduce exchange rates with other methods. Furthermore, the linear progression with time and direct concentration dependence suggest that exchange is limited by the rate of micelle-bubble interactions. CIE thus supports switchable entrapment with rapid exchange rates, supporting ongoing developments with kinetically controlled micelles.

■ INTRODUCTION

The dispersion of amphiphilic block copolymers in selective solvents leads to micellization. In micelles, the solvophobic blocks partition into a separate core phase to reduce contacts with the solvent phase, while the solvophilic blocks form a corona that maintains solvent contact. 1-4 The equilibrium diameter of a micelle is a balance of interfacial enthalpy with the entropy associated with chain stretching as well as other terms. In contrast, the actual diameter of a micelle is a combination of the processing history and the kinetics of chain exchange, in addition to thermodynamic considerations. Kinetically controlled micelles open new opportunities to decouple control of micelle size from subsequent uses. Current uses for kinetically controlled micelles span from nanoreactors and drug delivery to soft templates for functional materials.^{4–10} We note that such kinetically controlled micelles have various terms, including "nonergodic", "frozen micelles", "kinetically trapped", or "persistent micelles". The size distribution of kinetically controlled micelles are very sensitive to the preparation conditions 11-16 where homogenization and size tuning are inherently challenging.

Micelle equilibration via single chain exchange and fusion/ fission have been extensively studied. 12,17-24 Kinetic rates measured near equilibrium are usually attributed to single chain exchange (SCE)^{19,25} where there is a double-exponential

rate dependence on χN . Here the relevant χ term is between the solvent and the core block. Exchange rates measured far from equilibrium are not clearly consistent with a single mechanism, ^{22,31,32} but micelle fusion/fission is often considered.³³ The specific rates of exchange vary widely and can be unobservably slow. For example, prior SANS chain exchange measurements with both ~5.5 and ~8.5 kg/mol poly(ethylene oxide-b-butadiene) dispersed in water had negligible chain exchange when quiescent for 8 days.³⁰ Curiously, a related study with a similar 11.1 kg/mol poly(ethylene oxide-b-butadiene) found that the addition of stirring led to micelle size changes over an ~week time scale and resulted in a bimodal micelle size distribution.³⁴ Continuing with the same polymer, solution vortexing remarkably led to the complete mixing of chains within 15 min.³⁵ A new mechanism termed agitation induced chain exchange (AICE) was advanced where the continuous production of fresh solution-air interfacial area drove the adsorption of chains from micelles to the surface. The collapse of those fresh surfaces then released chains, bypassing the SCE rate-limiting step of chain extraction to the solvent. These

Received: June 10, 2018 Revised: August 14, 2018 Published: August 30, 2018

Department of Chemistry and Biochemistry, University of South Carolina, Columbia, South Carolina 29208, United States *Neutron Scattering Division and *The Center for Nanophase Materials Sciences (CNMS), Oak Ridge National Laboratory, Oak Ridge, Tennessee 37831, United States

Department of Chemical and Biomolecular Engineering, University of Tennessee, Knoxville, Tennessee 37934, United States

examples all have $\chi N \sim 200$ based on similar polybutadiene block molar masses and the reported χ value with water.³⁶ This collection of works shows that high- χN micelles can be either kinetically trapped when quiescent or have novel exchange mechanisms activated by agitation.

Cavitation induced exchange (CIE) recently emerged as a novel exchange mechanism during solution sonication. Here the use of ultrasonic waves induces continuous cavitation events with bubbles that grow and then implode rapidly on the microsecond time scale, capable of producing ephemeral conditions with more than a hundred atmospheres of pressure and temperatures more than 5000 K.37-39 Rapid cavitational implosions are considered adiabatic where the energy is localized over a limited spatial extent of ~50 nm.³⁹ Here, the rapid turnover of solution-gas interfaces from cavitation was previously shown to support tunable micelle size distributions using a high- χN system of poly(ethylene oxide-b-hexyl acrylate) (PEO-b-PHA) in THF/water mixtures. 40 When compared to solution vortexing, the same system exhibited an order of magnitude faster response to CIE as compared to solution vortexing. A mechanism was proposed for CIE where chains adsorbed on bubbles produced by cavitation and then upon rapid bubble collapse would insert into micelles. However, there have not yet been any direct measurements of high- χN chain exchange from CIE to evaluate the expected rate dependencies. We note that sonication has been used to induce micelle structure changes, 41-43 to break extended polymer assemblies^{44,45} and micellar aggregates,⁴⁶ and to disperse additives into micelles.⁴⁷⁻⁴⁹ Lastly, we note that ultrasonic absorption spectroscopy was used to study SCE rates for dynamic small-molecule surfactants. 50-54 To the best of our knowledge, polymer exchange has not yet been directly measured as a result of ultrasonic cavitation under kinetically controlled, high- χN conditions.

Small-angle neutron scattering (SANS) experiments using d/h-labeled polymers and contrast matched solvents are an established technique to measure chain exchange between micelles. 55,56 Micelles are prepared separately using either protonated or partially deuterated block copolymers. The solvent mixture is contrast matched to d/h-mixed micelles. Micelle solutions are prepared separately with each type of chain then aliquots of each type of micelle solution are combined (postmixed), yielding the maximum SANS contrast where subsequent mixing results in a decay of scattering intensity. The ultimate fully mixed state is obtained directly by mixing h- and d-labeled polymers prior to micellization to produce a reference sample (premixed). The extent of chain mixing is thus quantified by comparing progress from the initial postmixed state toward the final premixed state. Prior works examining SCE with quiescent solutions noted a log(time) dependence⁵⁷⁻⁶⁰ for extent of chain exchange whereas AICE was linear with time, 35 highlighting the active role of surface area production upon the extent of chain exchange. It was also observed that for both quiescent SCE and AICE during solution vortexing that the rate of exchange decreased with polymer concentration or homopolymer addition. 35,28,61 Here we find that the extent of chain exchange for CIE varies linearly with time, but its rate is remarkably enhanced with polymer concentration, overcoming the typical energetic barriers to other exchange processes.

EXPERIMENTAL METHODS

Materials. Poly(ethylene glycol) methyl ether (PEO-OH, M_n = 5000 g mol⁻¹, Aldrich), 2-bromopropionic acid (>99%, Aldrich), and 4-(dimethylamino)pyridine (99%, Aldrich) were used as received. The catalyst, copper(I) bromide (99.99%, Aldrich), ligand, tris[2-(dimethylamino)ethyl amine (97%, Aldrich), and anhydrous, inhibitor-free tetrahydrofuran (THF, 99% Aldrich) were stored inside a glovebox and used as received. Hexyl acrylate (96%, VWR) and deuterated hexyl acrylate-d₁₃ monomer were passed through basic alumina column just before use. Chloroform (>99%, Aldrich), hexane (>98.5%, Fisher), and dimethylformamide (97%, Aldrich) were used as received. Methanol (MeOH, 99.8%, Fisher) was dried at room temperature by storage over 30% w/v of molecular sieves (3 Å, 8-12 mesh, Acros Organics) for a week. Deuterium oxide (D₂O₂, 99.9% D) was purchased from Cambridge Isotopes and used as received. All reagents were used as received without any further purification unless otherwise stated. Dichloromethane, ethyl ether anhydrous, and magnesium sulfate anhydrous (Powder/Certified) were purchased from Fisher Scientific; hydroquinone (>99%) was received from TCI AMERICA; triethylamine (Et₃N, \geq 99%), 2,6-di-tert-butyl-4-methylphenol (BHT, ≥99%), and acryloyl chloride (≥96%) were obtained from Sigma-Aldrich; and *n*-hexanol (d_{13} , 98%; Lot I-15448) was purchased from Cambridge Isotopes Laboratories, Inc.

Hexyl- d_{13} Acrylate Synthesis and Characterization. Hydroquinone (1.0 g), BHT (1.0 g), 1-hexan-d₁₃-ol (5.0 g, 43.38 mmol), and Et₃N (18.1 mL, 130.14 mmol) were dissolved in dichloromethane (150 mL) under a nitrogen atmosphere and cooled in an ice bath with sodium chloride. A solution of acryloyl chloride (7.4 mL, 91.09 mmol) in 30 mL of dichloromethane was added dropwise to the stirred solution (Scheme S1). The reaction was allowed to warm to room temperature and was stirred overnight under nitrogen. Deionized water was then added, and the organic phase was collected. The aqueous phase was washed with dichloromethane $(3 \times 100 \text{ mL})$ to extract hexyl- d_{13} acrylate from the aqueous layer. Sequentially, the combined organic phases were dried over anhydrous MgSO₄. After adding 0.5 g of BHT and 0.5 g of hydroquinone, the solvent was removed by rotary evaporation to afford the crude product as a light yellow-green liquid. The final product was obtained by purification via column chromatography (1.5% ethyl ether in pentane) to yield a colorless liquid as the pure monomer (4.9 g, 67% yield). The monomer was stored with trace BHT/hydroquinone (1:1, 0.1 wt % of product), and stored frozen under nitrogen. ^IH and ¹³C NMR spectra were obtained on a Varian VNMRS 500 NMR spectrometer at 23 °C in CDCl₃ (7.27 ppm ¹H reference and 77.23 ppm ¹³C reference). Inverse-gated decoupling with a recycle delay of 25 s for ¹³C NMR spectra. ¹H NMR (CDCl₃): δ 6.39 (dd, J_{CD} = 17.4, 1.2 Hz, 1H, $CH_2=$), 6.11 (dd, $J_{CD}=17.4$, 10.5 Hz, 1H, =CH-), 5.80 (dd, $J_{CD}=$ 10.3, 1.0 Hz, 1H, CH₂=), 4.11 (s, residual -OCDH- integrating less than 1%), 1.61 (m, residual -OCD2CDH- integrating at about 12%), 1.32 (m, residual -CDHCDHCD3 integrating at about 4%). ¹³C{¹H} NMR (CDCl₃): δ 166.5 (CO), 130.6 (CH₂=CH₂-), 128.9 $(=CH_2-CO-)$, 64.2 (p, $J_{CD} = 22.4$ Hz, $-OCD_2-$ at $\sim 99\%$), 30.2 (p, $J_{\text{CD}} = 18.8 \text{ Hz}, -\text{OCD}_2\text{CD}_2\text{CD}_2\text{CD}_2$ at ~99%), 27.6 (p, $J_{\text{CD}} = 19.3$ Hz, −OCD₂CD₂− at ~87%; overlaps with triplet centered at 28.0 for $-OCD_2CDH-$ at $\sim 13\%$), 24.5 (p, $J_{CD} = 19.1$ Hz, $-OCD_2CD_2CD_2$ at ~99%), 21.4 (p, $J_{CD} = 19.1$ Hz, $-CD_2-CD_3$ at ~92%; overlaps with triplet centered at 21.7 for $-\text{CDH-CD}_3$ at \sim 8%), 13.0 (sept, J_{CD} = 19.1 Hz, $-CD_3$ at \sim 99%). See the ¹³C NMR spectrum in Figure S1.

Block Copolymer Synthesis and Characterization. A poly-(ethylene oxide-b-hexyl acrylate), PEO-b-PHA, diblock copolymer was synthesized along with a corresponding deuterated analogue, PEO-b-dPHA. The two-step synthesis started with a Steglich esterification of poly(ethylene glycol) methyl ether, followed by atom transfer radical polymerization (ATRP) as described elsewhere in detail. PEO₄₅₄-b-PHA₈₅ and PEO₄₅₄-b-dPHA₈₂, where the subscripts denote degree of polymerization, were synthesized from the same PEO macroinitiator ($M_{\rm n} = 5~{\rm kg~mol}^{-1}$, D = 1.06). The molar mass of PHA growth was determined using a Bruker Avance III HD 300 1 H NMR by comparison to the known PEO. The dPHA similarly

contained backbone protons for determination of molar mass by $^1\mathrm{H}$ NMR. The molar mass dispersity (\mathcal{D}) was characterized using a Varian gel permeation chromatograph (GPC) equipped with a Shimadzu 20AD LC pump, three styragel columns (HR1, HR3, and HR4 in the effective molecular weight range of 0.1–5, 0.5–30, and 5–600 kg mol $^{-1}$, respectively), and a Varian 390-LC refractive index detector. The GPC was calibrated with poly(methyl methacrylate) standards (2.8, 5.0, 10.3, 27.6, 60.2, 138.6, 342.9, and 625.5 kg mol $^{-1}$) obtained from Polymer Laboratories. GPC samples were prepared in THF at a concentration of 4 mg mL $^{-1}$, filtered through a 0.2 $\mu\mathrm{m}$ syringe filter prior to injection. PEO-b-PHA ($M_\mathrm{n}=18.4~\mathrm{kg}~\mathrm{mol}^{-1}$, $\mathcal{D}=1.10$) and PEO-b-dPHA ($M_\mathrm{n}=18.8~\mathrm{kg}~\mathrm{mol}^{-1}$, $\mathcal{D}=1.18$) both had hydrophobic weight fractions of 0.73 (Figures S2).

Micelle Preparation. Four different polymer concentrations were prepared for each set of solutions described: 1.0, 0.5, 0.2, and 0.1 wt %. Premixed solutions were prepared by thorough mixing of 50 wt % dried PEO-b-PHA and 50 wt % dried PEO-b-dPHA in THF, a neutral solvent for both blocks. The THF was removed by heating at 60 °C for \sim 3 h until complete dryness. This random mixture of 50/50 wt % PHA/dPHA was then dispersed in MeOH followed by dropwise addition of D₂O to a composition of 51 vol % MeOH/49 vol % D₂O mixture. The solvent composition was designed to match the contrast of the mixed core⁶² and had a measured density of 1.00 g/mL. In addition, two separate solutions were prepared containing either PEO-b-PHA or PEO-b-dPHA by first dispersing the polymer in MeOH followed by dropwise D₂O addition to the same composition as above with gentle inversion. Subsequently, equal volume aliquots from each h/d solution were combined and sonicated in a Fisher ultrasonic bath (Cat. no. FS-28) operated continuously at full power (225 W) and frequency of 40 kHz for prescribed times, maintaining temperature between 20-30 °C with ice additions, prior to SANS measurement (postmixed, variable t_{CIE}). Quiescent solutions were subsequently remeasured to quantify for chain exchange in the absence of sonication.

SANS Measurements. Micelle solutions were measured in quartz Hellma cells with a path length of 1 mm. SANS experiments were performed on the CG-2 General Purpose SANS instrument at the High Flux Isotope Reactor at Oak Ridge National Laboratory. A nincident neutron wavelength (λ) of 4.75 Å was used with a sample-to-detector distance of 7 m to acquire a *q*-range from 0.008 Å⁻¹ < *q* < 0.2 Å⁻¹. The SANS data were acquired for 15 min with a flux of ~9 M neutrons per second incident upon the sample. All measurements were performed at 20 °C. The data were reduced using a custom IGOR Pro software package from ORNL. Data were corrected for background scattering using detector sensitivity, empty cell scattering, sample thickness, and sample transmission. Scattering intensities are presented on an absolute scattering intensity scale.

SANS Analysis. The extent of chain exchange was monitored by the changing scattering intensity over the range $0.01 \le q \le 0.03 \text{ Å}^{-1}$. Exchange was quantified using a relaxation function, $R(t_{\text{CIE}})$: ⁵⁷

$$R(t_{\text{CIE}}) = \left(\frac{I(t_{\text{CIE}}) - I(\infty)}{I(0) - I(\infty)}\right)^{1/2} \tag{1}$$

where $I(\infty)$ is the intensity for the premixed solution and I(0) and $I(t_{\text{CIE}})$ are the intensities for the solution at a given mixed aliquots (time 0 and sonicated times thereafter). Here an absence of chain exchange corresponds to $R(t_{\text{CIE}})=1.0$, and complete mixing corresponds to $R(t_{\text{CIE}})=0$. The premixed reference sample $(I(\infty))$ is necessary since the fully mixed micelles do not result in a zero-contrast condition due to residual scattering from e.g. core—corona contrast. The $R(t_{\text{CIE}},q)$ values were calculated for each measured q from 0.01 to 0.03 Å $^{-1}$. The reported $R(t_{\text{CIE}})$ values were calculated as the average of all these $R(t_{\text{CIE}},q)$ values for each treatment to improve the signal-to-noise. The $R(t_{\text{CIE}})$ analysis was constrained to the q-region from 0.01 to 0.03 Å $^{-1}$ where there was maximum scattering intensity to minimize detection error (Poisson). The uncertainty in $R(t_{\text{CIE}})$ was calculated by propagating the uncertainty from the measured scattering intensity and the uncertainty of polymer

concentration. Slopes were fitted using a least-squares optimization, and the standard errors were reported.

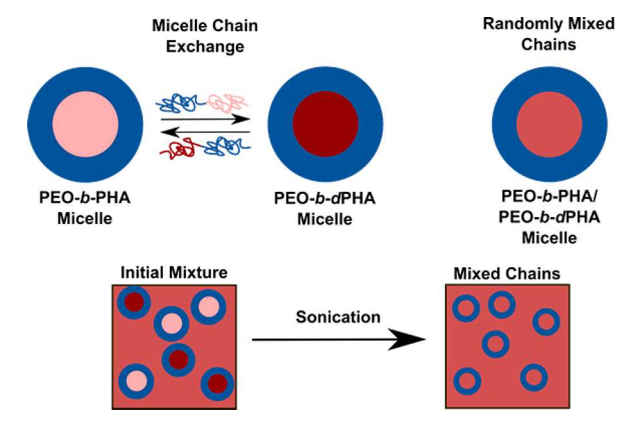
GPC after Sonication. GPC measurements of polymers as a function of sonication time were conducted at 1.0 wt % to mimic experimental conditions with PEO-b-PHA. Solutions were prepared by polymer dispersion in MeOH followed by dropwise addition of $\rm H_2O$ to a 51 vol % MeOH/49 vol % $\rm H_2O$ composition with slight mixing. Aliquots were divided into equal volumes and subjected to ultrasonic cavitation for various times. Following sonication, the solvents were evaporated on a hot plate at 40 °C for 3 h. GPC samples were then prepared in THF at 10 mg/mL and filtered through a 0.2 μ m syringe filter prior to injection.

DLS after Sonication. The hydrodynamic diameter of micelles in solution as a function of sonication time was measured using dynamic light scattering (DLS). PEO-b-PHA was dispersed in MeOH/H2O similarly as for SANS studies. Aliquots of 2 mL were filtered through $0.2 \mu m$ syringe filters into polystyrene cuvettes and were tightly sealed. Measurements were obtained using a Zetasizer Nanoseries ZEN3690 instrument. DLS measurements were taken at time zero, without sonication. The same cuvette was exposed to ultrasonic cavitation with $t_{\text{CIE}} = 10-300$ min with periodic DLS measurements. Similar to the SANS studies, the ultrasonic bath was maintained between 20 and 30 $^{\circ}\text{C}$ with ice additions. Measurements were run at 25 °C with 10 min thermal equilibration time prior to each 10 min acquisition. The data were analyzed using a solvent mixture viscosity of 0.547 cP and refractive index (RI) of 1.326 calculated using pure water and MeOH values and the mole fraction.^{65,66} A log-normal distribution was fit for each measurement corresponding to the mean and standard deviation reported in Table S1.

RESULTS AND DISCUSSION

Chain exchange was examined when quiescent and as a result of sonication using contrast matched SANS experiments (Scheme 1 and Figure 1). Postmixed micelle solutions were

Scheme 1. Representation of Contrast Conditions during SANS Measurements.^a



^aMicelles are prepared separately with either d/h-labeled chains. The solutions are combined (postmixed) in a solvent that is contrast matched to a randomly mixed micelle core. The initial mixture has maximum scattering contrast where ultrasonic cavitation results in chain mixing and decreased scattering contrast.

first examined for chain exchange under quiescent conditions (Figure S3). Time-resolved measurements were not necessary since scattering curves for quiescent samples were constant for extended periods, up to 12 h checked, indicating a lack of detectable chain exchange. This observation confirms that the χN conditions here are sufficiently high to arrest chain exchange on the experimental time scale. Again, the pertinent χ parameter for micelle formation and chain exchange is between

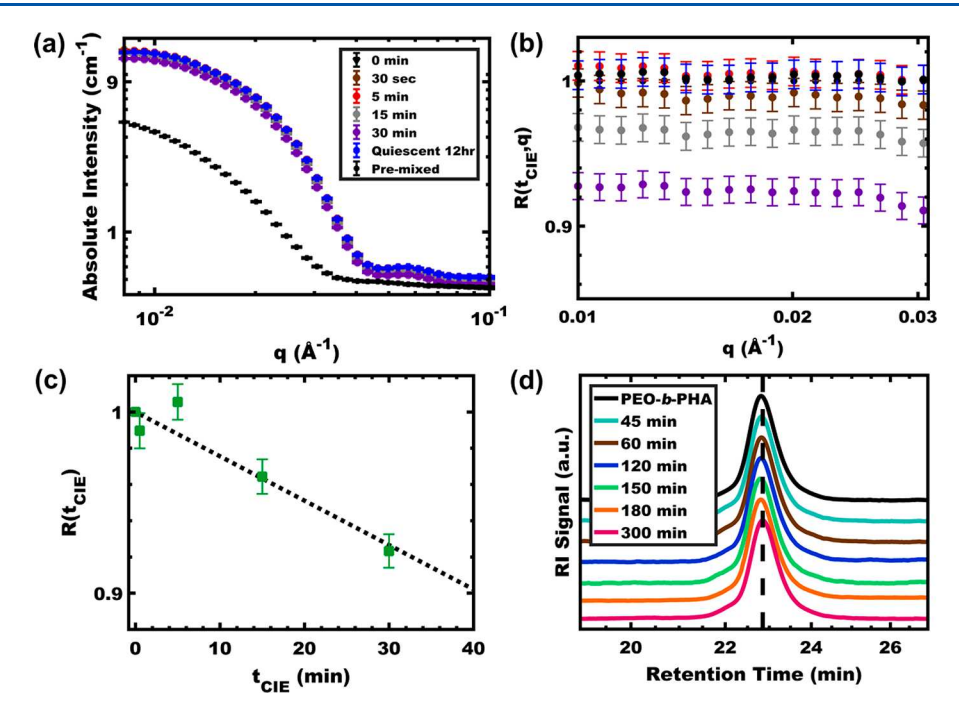
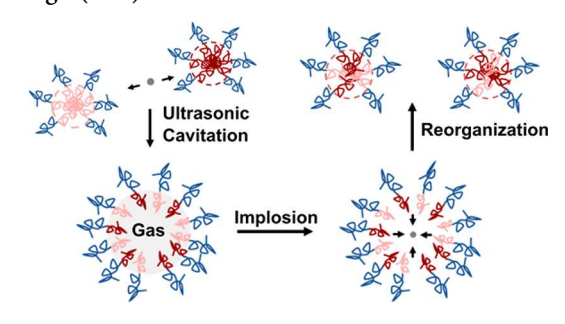


Figure 1. SANS data of 1.0 wt % micelle solutions with different treatments (a). The relaxation function $R(t_{\rm CIE})$ was averaged over a q-range for improved signal-to-noise (b). The resulting average $R(t_{\rm CIE})$ was calculated for each sonication time (c). GPC measurements of the same protonated polymer subjected to extensive sonication (d). The GPC data in (d) were offset vertically for clarity. Error bars in (a) correspond to the standard deviation of the measured scattering intensity. Error bars in (b, c) correspond to uncertainty propagated from both the measured intensity and the polymer concentration.

the core forming block (PHA) and the solvent system (MeOH–water). Solubility parameters were found to provide an unrealistic estimate for $\chi_{\rm PHA-MeOH/water} \sim 28.6$. For comparison, polybutadiene, a similarly hydrophobic block, has experimentally measured values of $\chi_{\rm PB-water} \sim 3.5$ and $\chi_{\rm PB-MeOH} \sim 3.3$. Based on these closest available comparisons, the present experiments are estimated to have $\chi N \sim 500$. Thus, the present experiments are anticipated to be deeply trapped with more than twice the χN barrier as recent kinetically controlled PEO-*b*-PB/water experiments.

SANS of postmixed micelles was also measured as a function of sonication time. The posited mechanism for CIE is that cavitational implosions drive chain exchange by enabling chain extraction to ephemeral cavitation bubbles followed by bubble collapse and rapid chain integration into micelles (Scheme 2). Here the rate of cavitational implosions is constant during ultrasonication and is expected to lead to a linear decrease in the relaxation function $R(t_{CIE})$. The data for 1.0 wt % solutions are shown in Figure 1A where the scattering intensity monotonically decreased with sonication time. The relaxation function $R(t_{CIE},q)$ was calculated over a range of q-values $(0.01-0.03 \text{ Å}^{-1})$ and was then averaged to improve the signalto-noise (Figure 1B). The scattering intensity was highest in this q-range, and the calculated $R(t_{CIE},q)$ values were invariant with q. The average $R(t_{CIE})$ values with sonication time are shown in Figure 1C. We note that this common method has been shown to yield nearly identical results to an alternative approach that integrates intensity over the same range.²⁶⁻²⁸ This $R(t_{CIE})$ trend is the first direct observation of high- χN chain exchange during CIE. The linear progression of $R(t_{\rm CIE})$ with time suggests that the exchange process is limited by the extent of ultrasonic cavitation. A commonplace laboratory ultrasonic bath was used where these procedures are easily employed in diverse laboratories. A similar linear dependence

Scheme 2. Posited Mechanism for Cavitation Induced Exchange (CIE).^a



"Ultrasonic induced cavitation creates fresh solution—gas interface that adsorbs polymer chains. The subsequent rapid implosion of the bubble releases free chains that quickly integrate into micelles. The rate of micelle—bubble interactions is expected to limit the rate of exchange. This exchange rate is expected to be constant with time and directly proportional to the polymer concentration.

with vortex time was noted for the surface-limited exchange process in AICE. In contrast, SCE typically progresses with a linear dependence of $R(t_{\rm SCE})$ with log(time) $^{57-60}$ as a result of the combination of the original Halperin and Alexander model core block dispersity. The $R(t_{\rm CIE})$ calculation assumes constant form factor where the micelle dimension is constant, and thus changes to intensity are attributed to chain mixing alone. Because CIE is used far from equilibrium, we focused on early mixing times with a limited extent of mixing having $R(t_{\rm CIE}) > 0.9$ where both DLS measurements of overall hydrodynamic diameter (Table S1 and Figure S4) and SANS form factor fitting for the spherical PHA core (Table S2 and Figure S5) confirmed that the nominal micelle dimensions were not observably changed when $R(t_{\rm CIE}) > 0.9$. Analysis was

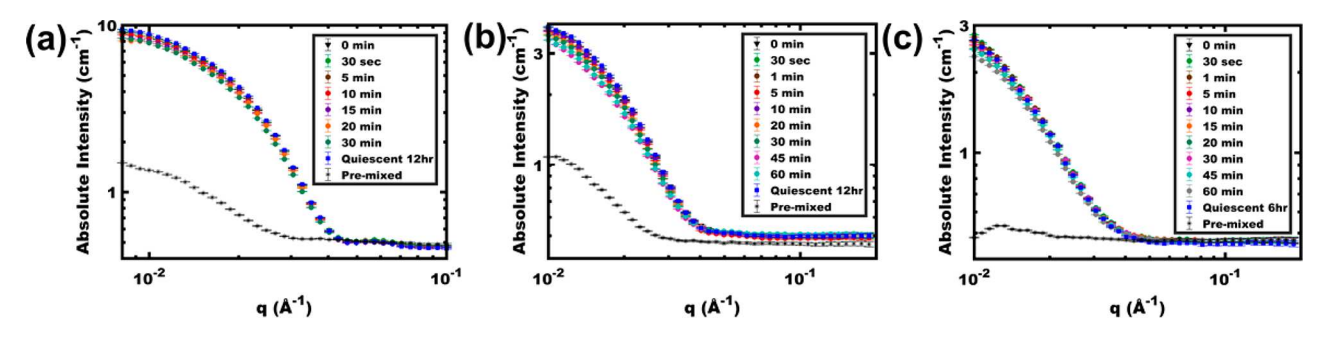


Figure 2. SANS data with different treatments for 0.5, 0.2, and 0.1 wt % micelle solutions, (a), (b), and (c), respectively. Error bars represent standard deviation in measured scattering intensity.

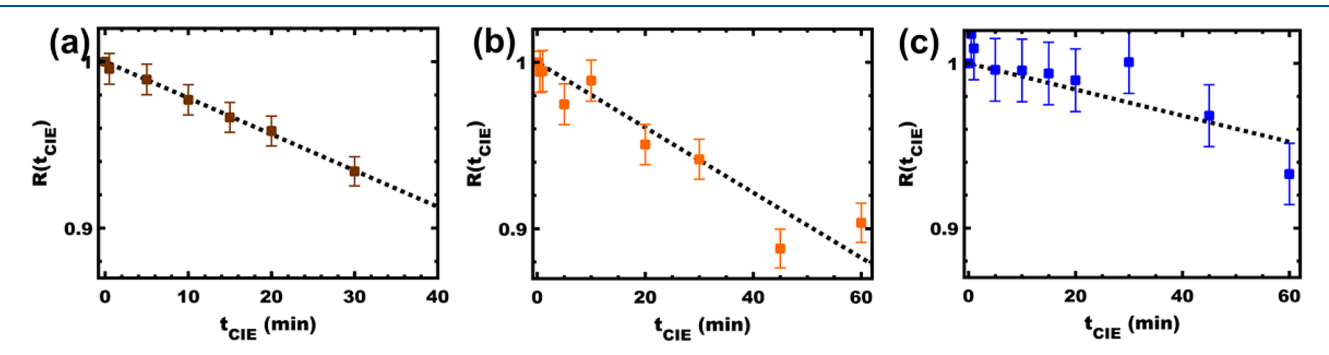


Figure 3. Average relaxation function $R(t_{\text{CIE}})$ with sonication time for 0.5, 0.2, and 0.1 wt % micelle solutions, (a), (b), and (c), respectively. Error bars correspond to uncertainty propagated from both the measured intensity and the polymer concentration.

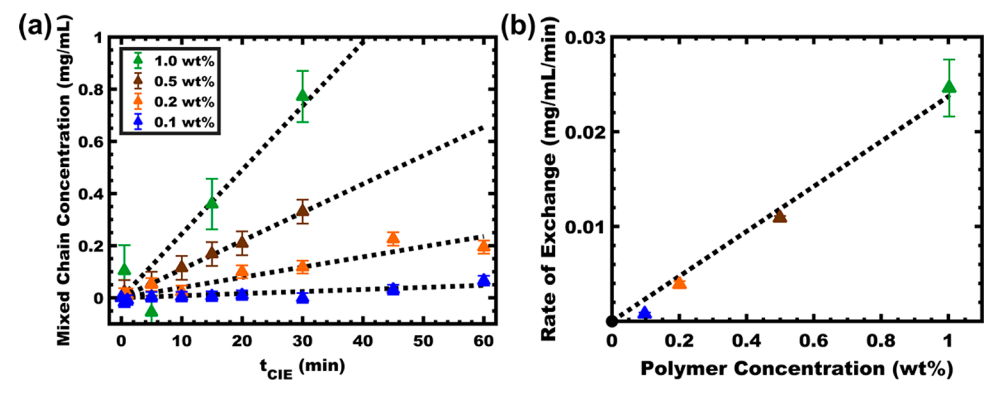


Figure 4. Mixed chain concentration increased linearly with time for all concentrations examined (a). The rate of chain exchange was directly proportional to the polymer concentration (b). Error bars in (a) correspond to uncertainty propagated from both the measured intensity and the polymer concentration. Error bars in (b) correspond to standard error from least-squares fitting.

thus constrained to low mixing extents with $R(t_{\rm CIE})$ > 0.9 to minimize contributions from size changes⁶⁹ which were observed by DLS only after more extended sonication times (Table S1). The original works of Halperin and Alexander predicted that chain exchange would progress faster than changes to the nominal micelle size. 19 Sonication has been noted to produce reactive solvent radicals³⁹ and the harsh conditions have been noted to degrade high molar mass polymers. 70-73 To check for chain degradation, we conducted GPC measurements on PEO-b-PHA as a function of sonication time under identical conditions (Figure 1d). GPC measurements did not detect any change in the molar mass distribution nor the appearance of low molar mass contaminants as a result of sonication, up to the maximum time point checked of 5 h. This 5 h sonication time was without observable changes to the polymer and far exceeds the durations used here for SANS exchange measurements. Thus,

the interpreted chain exchange from intensity changes cannot be attributed to degradation of the polymers.

SANS experiments were conducted at multiple concentrations ranging from 0.1 to 1.0 wt % to gain insights into the underlying mechanism. The rate of chain exchange for the posited CIE mechanism is expected to scale directly with polymer concentration due to an increased probability of micelle—bubble interactions. Figure 2 presents the SANS data from sonication time variation for 0.1–0.5 wt % polymer solutions. Performing the same $R(t_{\rm CIE})$ analysis within the limit of $R(t_{\rm CIE}) > 0.9$ led again to linear $R(t_{\rm CIE})$ relationships with CIE time for all concentrations examined (Figure 3). The fluctuations in $R(t_{\rm CIE})$ about the nominally linear trend are consistent with the propagated uncertainty. For each concentration data set, the expected constant rate of mixing is the simplest interpretation; however, we cannot exclude the possibility of an induction time due to the calculated

uncertainty. This further supports that the exchange process is limited by the extent of cavitation for a range of concentrations. Again, the assumption of constant micelle size for $R(t_{CIF})$ calculations was checked by DLS measurements and SANS form factor fitting where much longer sonication times were needed to induce observable changes (Figures S4 and S5, Tables S1 and S2). Here, lower polymer concentrations required further extended sonication times to reach similar extents of mixing. For example, the 1.0 wt % sample reach $R(t_{CIE}) = 0.95$ after 20 min of sonication, whereas the 0.5, 0.2, and 0.1 wt % samples required 23, 26, and 63 min of sonication, respectively, as extrapolated from the linear best fits. The mass flow associated with chain exchange may be calculated by assuming the process follows a zero-order rate expression. Here the quantity $[1 - R(t_{CIE})]$ represents the fraction of chains exchanged, and $c_0[1 - R(t_{\rm CIE})]$ represents the concentration of mixed chains where c_0 is the constant polymer concentration. Using this approach, the concentration of mixed chains may be examined as a function of time and polymer concentration. It was found that the concentration of mixed chains increased linearly with time for all concentrations (Figure 4A). The slopes from the resulting linear fits yielded the corresponding zero-order rate constants (Table 1). Comparison of the resulting slopes indicates that the rate of chain exchange increased with polymer concentration.

Table 1. Rate Constants for CIE with Different Polymer Concentrations

polymer concn (wt %)	polymer concn (mg/mL)	rate const (mg/mL/min)	R^2
0.10	0.977	$7.8 \times 10^{-4} \pm 1.5 \times 10^{-4}$	0.708
0.20	2.01	$3.9 \times 10^{-3} \pm 3.2 \times 10^{-4}$	0.895
0.50	5.01	$1.1 \times 10^{-2} \pm 2.0 \times 10^{-4}$	0.995
1.0	10.1	$2.5 \times 10^{-2} \pm 3.0 \times 10^{-3}$	0.910

The increased rate of chain exchange for CIE with polymer concentration is remarkable. Prior works with SCE identified that the rate of exchange was relatively constant for low concentrations of 0.5-2 vol %²⁹ but was considerably reduced with high concentrations of 15 vol %61 or the addition of homopolymer.²⁸ Here additional overlap of corona blocks was theoretically predicted to increase the activation energy for SCE.²⁴ Similarly, prior works with AICE using vortexing found that the rate of exchange was similar for low concentrations (~0.24-0.75 wt %) but reduced considerably with higher concentrations (~1.0-1.5 wt %).35 It was speculated that the energetic penalty for chain exchange increased when approaching the semidilute regime, corresponding to a marked decrease in the observed exchange rate. Admittedly, the concentrations employed in this study are within the dilute regime but are close to the semidilute regime. Regardless, the concentrations examined here are commensurate with these comparable works. In contrast, the rate of exchange for CIE increased with polymer chain concentration, even upon approaching the semidilute regime (~1.0 wt %). This trend is counter to that expected based upon corona overlap, counter to that expected based upon viscosity, and counter to observations of slowed surfactant and nanoparticle adsorption to air-liquid interfaces with concentration. 74,75 A possible explanation for the observed CIE trend is that cavitational implosions provide an energy that exceeds these energetic barriers for chain exchange. Another possible explanation is that the rapid microsecond time scale for cavitation results in a low surface excess without sufficient time to produce a surfactant surface coverage that inhibits further adsorption.

Further insights into the CIE mechanism are found by quantitatively examining the rate dependence upon polymer concentration (Figure 4B). The posited mechanism for CIE (Scheme 2) is that cavitational implosions drive the extraction of chains from micelles. Ultrasonic cavitation in the presence of surfactants is known to reduce bubble coalescence, 76-78 and this apparent surface activity of surfactants during ultrasonic cavitation suggests that adsorption processes are active during rapid cavitation events. After chain extraction, bubble implosion is expected to cause the extracted chains to rapidly integrate into micelles. The surface velocities of cavitational implosions can be quite rapid, exceeding ~1 m/s.⁷⁹ This solution-gas wavefront thus passes across a volume of solution, displacing micelles along the way. The rate of micelle-bubble interactions and thus the rate of chain exchange are expected to be proportional to the polymer concentration as long as the available energy enables efficient chain extraction. The present data are well fitted by a directly proportional relationship for chain exchange rate with polymer concentration. Here the rate of exchange (mg/mL/min) = $0.024 \pm 9.5 \times 10^{-4} \text{ (mg/mL/min/wt \%)} \times \text{polymer}$ concentration (wt %) with a Pearson's correlation coefficient of $R^2 = 0.989$. The above arguments provide a possible explanation for the proportional acceleration of CIE with polymer concentration. However, we note that many questions remain open about the CIE mechanism. Chain exchange may occur via extraction of chains to the cavitation surface, although we cannot exclude micelle fusion/fission that could e.g. be driven by the collision of adsorbed micelles 80,81 during bubble implosion. Chain extraction might occur during bubble growth, bubble collapse, or both. Also, each micelle-bubble interaction may remove a small fraction of chains or may rip the entire micelle apart into adsorbed unimers. Here questions of molecular level interactions with ultrasonic waves could benefit from future computational studies. It is not clear whether CIE drives micelle size equilibration or rather produces a distinct distribution based upon kinetic entrapment. Lastly, the dependence of CIE rate on χ , N, bubble lifetime ⁸² (frequency dependent), bubble size ^{76,83} (frequency and solvent dependent), bubble velocity⁷⁹ (power dependent), and cavitation mode⁸² (transient vs stable, dissolved gas dependent) are interesting parameters for further research. While many questions remain open, the data here show that CIE drives initial chain exchange at a constant rate that is directly proportional to the polymer concentration.

CONCLUSIONS

This study utilized contrast-matched SANS techniques to examine the cavitation induce exchange of polymer chains between high- χN micelles. Concentrations were examined from 0.1 to 1.0 wt % as a function of sonication time. The examined micelle solutions were estimated to have $\chi N \sim 500$ and were confirmed to have unobservable chain exchange when quiescent. In all cases, the extent of chain exchange progressed linearly with time, suggesting that exchange is limited by the extent of ultrasonic cavitation. The rate of chain mixing was found to be directly proportional to the polymer

concentration as predicted by the posited mechanism. This suggests that the typical energetic barriers for chain exchange are exceeded by the available energy from CIE. This unique concentration-based acceleration of exchange under high- χN conditions may enable concentrated industrial processing of kinetically controlled micelles dispersed in highly selective solvents.

ASSOCIATED CONTENT

S Supporting Information

The Supporting Information is available free of charge on the ACS Publications website at DOI: 10.1021/acs.macromol.8b01244.

Scheme and ¹³C NMR of hexyl- d_{13} acrylate monomer, ¹H NMR and GPC of PEO-*b*-PHA and PEO-*b*-*d*PHA, additional quiescent SANS data, DLS data, and SANS form factor fitting (PDF)

AUTHOR INFORMATION

Corresponding Author

*(M.S.) E-mail: morgan@stefikgroup.com.

ORCID ®

Kayla A. Lantz: 0000-0002-9128-0786 Kunlun Hong: 0000-0002-2852-5111 Morgan Stefik: 0000-0002-2645-7442

Present Address

[#]Department of Chemical and Biological Engineering, Rensselaer Polytechnic Institute, Troy, NY 12180.

Notes

The authors declare no competing financial interest.

ACKNOWLEDGMENTS

Morgan Stefik acknowledges support by the National Science Foundation under NSF award #DMR-1752615. Hexyl-d₁₃ acrylate was synthesized and characterized at the Center for Nanophase Materials Sciences, which is a DOE Office of Science User Facility. This work made use of resources at the High Flux Isotope Reactor, a DOE Office of Science User Facility operated by the Oak Ridge National Laboratory. Kayla A. Lantz acknowledges partial support by the National Science Foundation EPSCoR Program under NSF Award #OIA-1655740 and partial support from NSF Award #DMR-1752615. We thank Dr. Elizabeth Kelley for helpful SANS discussions, Zachary Marsh for polymer synthesis discussions, Benjamin Lamm for MatLab assistance, and Wessel van den Bergh for statistics discussions.

REFERENCES

- (1) Beck, J. S.; Vartuli, J. C.; Roth, W. J.; Leonowicz, M. E.; Kresge, C. T.; Schmitt, K. D.; Chu, C. T.-W.; Olson, D. H.; Sheppard, E. W.; Mccullen, S. B. A New Family of Mesoporous Molecular Sieves Prepared with Liquid Crystal Templates. *J. Am. Chem. Soc.* **1992**, *114*, 10834–10843.
- (2) Honda, C.; Hasegawa, Y.; Hirunuma, R.; Nose, T. Micellization Kinetics of Block Copolymers in Selective Solvent. *Macromolecules* **1994**, 27 (26), 7660–7668.
- (3) Zhang, L.; Eisenberg, A. Multiple Morphologies of "Crew-Cut" Aggregates of Polystyrene-b-Poly(Acrylic Acid) Block Copolymers. *Science* **1995**, 268 (5218), 1728–1731.
- (4) Alexandridis, P.; Lindman, B. Amphiphilic Block Copolymers: Self-Assembly and Applications; Elsevier: 2000.

(5) Vriezema, D. M.; Comellas Aragonès, M.; Elemans, J. A. A. W.; Cornelissen, J. J. L. M.; Rowan, A. E.; Nolte, R. J. M. Self-Assembled Nanoreactors. *Chem. Rev.* **2005**, *105* (4), 1445–1490.

- (6) Lavasanifar, A.; Samuel, J.; Kwon, G. S. Poly(Ethylene Oxide)-Block-Poly(L-Amino Acid) Micelles for Drug Delivery. *Adv. Drug Delivery Rev.* **2002**, *54*, 169–190.
- (7) Lokupitiya, H. N.; Jones, A.; Reid, B.; Guldin, S.; Stefik, M. Ordered Mesoporous to Macroporous Oxides with Tunable Isomorphic Architectures: Solution Criteria for Persistent Micelle Templates. *Chem. Mater.* **2016**, 28 (6), 1653–1667.
- (8) Peters, K.; Lokupitiya, H. N.; Sarauli, D.; Labs, M.; Pribil, M.; Rathouský, J.; Kuhn, A.; Leister, D.; Stefik, M.; Fattakhova-Rohlfing, D. Nanostructured Antimony-Doped Tin Oxide Layers with Tunable Pore Architectures as Versatile Transparent Current Collectors for Biophotovoltaics. *Adv. Funct. Mater.* **2016**, *26* (37), 6682–6692.
- (9) Sarkar, A.; Stefik, M. How to Make Persistent Micelle Templates in 24 h and Know It Using X-Ray Scattering. *J. Mater. Chem. A* **2017**, 5 (23). 11840–11853.
- (10) Sarkar, A.; Evans, L.; Stefik, M. Expanded Kinetic Control for Persistent Micelle Templates with Solvent Selection. *Langmuir* **2018**, 34 (20), 5738–5749.
- (11) Cameron, N. S.; Corbierre, M. K.; Eisenberg, A. 1998 E.W.R. Steacie Award Lecture Asymmetric Amphiphilic Block Copolymers in Solution: A Morphological Wonderland. *Can. J. Chem.* 1999, 77 (8), 1311–1326.
- (12) Hayward, R. C.; Pochan, D. J. Tailored Assemblies of Block Copolymers in Solution: It Is All about the Process. *Macromolecules* **2010**, 43 (8), 3577–3584.
- (13) Riess, G. Micellization of Block Copolymers. *Prog. Polym. Sci.* **2003**, 28 (7), 1107–1170.
- (14) Lutz, J.-F. Solution Self-Assembly of Tailor-Made Macromolecular Building Blocks Prepared by Controlled Radical Polymerization Techniques. *Polym. Int.* **2006**, *55* (9), 979–993.
- (15) Choucair, A.; Éisenberg, A. Control of Amphiphilic Block Copolymer Morphologies Using Solution Conditions. *Eur. Phys. J. E: Soft Matter Biol. Phys.* **2003**, *10*, 37–44.
- (16) Gaucher, G.; Dufresne, M.-H.; Sant, V. P.; Kang, N.; Maysinger, D.; Leroux, J.-C. Block Copolymer Micelles: Preparation, Characterization and Application in Drug Delivery. *J. Controlled Release* **2005**, *109*, 169–188.
- (17) Owen, S. C.; Chan, D. P. Y.; Shoichet, M. S. Polymeric Micelle Stability. *Nano Today* **2012**, *7*, 53–65.
- (18) Rharbi, Y.; Li, M.; Winnik, M. A.; Hahn, K. G. Temperature Dependence of Fusion and Fragmentation Kinetics of Triton X-100 Micelles. *J. Am. Chem. Soc.* **2000**, *122* (26), 6242–6251.
- (19) Halperin, A.; Alexander, S. Polymeric Micelles: Their Relaxation Kinetics. *Macromolecules* **1989**, 22 (5), 2403–2412.
- (20) Mai, Y.; Eisenberg, A. Self-Assembly of Block Copolymers. Chem. Soc. Rev. 2012, 41 (18), 5969.
- (21) Nicolai, T.; Colombani, O.; Chassenieux, C. Dynamic Polymeric Micelles versus Frozen Nanoparticles Formed by Block Copolymers. *Soft Matter* **2010**, *6* (14), 3111.
- (22) Denkova, A. G.; Mendes, E.; Coppens, M.-O. Non-Equilibrium Dynamics of Block Copolymer Micelles in Solution: Recent Insights and Open Questions. *Soft Matter* **2010**, *6* (11), 2351.
- (23) Patist, A.; Kanicky, J. R.; Shukla, P. K.; Shah, D. O. Importance of Micellar Kinetics in Relation to Technological Processes. *J. Colloid Interface Sci.* **2002**, 245 (1), 1–15.
- (24) Halperin, A. On Micellar Exchange: The Role of the Insertion Penalty. *Macromolecules* **2011**, 44 (13), 5072–5074.
- (25) Nyrkova, I. A.; Semenov, A. N. On the Theory of Micellization Kinetics. *Macromol. Theory Simul.* **2005**, *14* (9), 569–585.
- (26) Lu, J.; Bates, F. S.; Lodge, T. P. Remarkable Effect of Molecular Architecture on Chain Exchange in Triblock Copolymer Micelles. *Macromolecules* **2015**, *48* (8), 2667–2676.
- (27) Lu, J.; Bates, F. S.; Lodge, T. P. Chain Exchange in Binary Copolymer Micelles at Equilibrium: Confirmation of the Independent Chain Hypothesis. *ACS Macro Lett.* **2013**, *2* (5), 451–455.

(28) Lu, J.; Bates, F. S.; Lodge, T. P. Addition of Corona Block Homopolymer Retards Chain Exchange in Solutions of Block Copolymer Micelles. *Macromolecules* **2016**, *49* (4), 1405–1413.

- (29) Choi, S.-H.; Lodge, T. P.; Bates, F. S. Mechanism of Molecular Exchange in Diblock Copolymer Micelles: Hypersensitivity to Core Chain Length. *Phys. Rev. Lett.* **2010**, *104* (4), 047802.
- (30) Won, Y.-Y.; Davis, H. T.; Bates, F. S. Molecular Exchange in PEO-PB Micelles in Water. *Macromolecules* **2003**, *36* (3), 953-955.
- (31) Meli, L.; Lodge, T. P. Equilibrium vs Metastability: High-Temperature Annealing of Spherical Block Copolymer Micelles in an Ionic Liquid. *Macromolecules* **2009**, *42*, 580–583.
- (32) Rharbi, Y. Fusion and Fragmentation Dynamics at Equilibrium in Triblock Copolymer Micelles. *Macromolecules* **2012**, *45* (24), 9823–9826.
- (33) Dormidontova, E. E. Micellization Kinetics in Block Copolymer Solutions: Scaling Model. *Macromolecules* **1999**, *32* (22), 7630–7644.
- (34) Kelley, E. G.; Murphy, R. P.; Seppala, J. E.; Smart, T. P.; Hann, S. D.; Sullivan, M. O.; Epps, T. H., III. Size Evolution of Highly Amphiphilic Macromolecular Solution Assemblies via a Distinct Bimodal Pathway. *Nat. Commun.* **2014**, *5*, 3599.
- (35) Murphy, R. P.; Kelley, E. G.; Rogers, S. A.; Sullivan, M. O.; Epps, T. H. Unlocking Chain Exchange in Highly Amphiphilic Block Polymer Micellar Systems: Influence of Agitation. *ACS Macro Lett.* **2014**, *3* (11), 1106–1111.
- (36) Michalek, S. Determination of a Polymer-Sorbate Interaction Parameter by a Sorption Method. *Zesz. Nauk. Politech. Krakow. Chem.* **1977**, 9 (10), 37.
- (37) Suslick, K. S. The Temperature of Cavitation. *Science* **1991**, 253 (5026), 1397–1399.
- (38) Suslick, K. S.; Flannigan, D. J. Inside a Collapsing Bubble: Sonoluminescence and the Conditions During Cavitation. *Annu. Rev. Phys. Chem.* **2008**, *59*, 659–683.
- (39) Cravotto, G.; Cintas, P. Power Ultrasound in Organic Synthesis: Moving Cavitational Chemistry from Academia to Innovative and Large-Scale Applications. *Chem. Soc. Rev.* **2006**, 35 (2), 180–196.
- (40) Lokupitiya, H. N.; Stefik, M. Cavitation-Enabled Rapid and Tunable Evolution of High-XN Micelles as Templates for Ordered Mesoporous Oxides. *Nanoscale* **2017**, 9 (4), 1393–1397.
- (41) Yusof, M.; Ashokkumar, M. Ultrasonic Transformation of Micelle Structures: Effect of Frequency and Power. *Ultrason. Sonochem.* **2015**, *24*, 8–12.
- (42) Cai, S.; Vijayan, K.; Cheng, D.; Lima, E. M.; Discher, D. E. Micelles of Different Morphologies—Advantages of Worm-like Filomicelles of PEO-PCL in Paclitaxel Delivery. *Pharm. Res.* **2007**, 24 (11), 2099–2109.
- (43) Zhang, Y.; Li, H.; Liu, Y.-Q.; Wang, J. Sonochemical Synthesis and Liquid Crystal Assembly of PS-b-PEO—titania Aggregates. *Chem. Commun.* **2012**, *48* (68), 8538.
- (44) Wang, X.; Liu, K.; Arsenault, A. C.; Rider, D. A.; Ozin, G. A.; Winnik, M. A.; Manners, I. Shell-Cross-Linked Cylindrical Polyisoprene-b-Polyferrocenylsilane (PI-b-PFS) Block Copolymer Micelles: One-Dimensional (1D) Organometallic Nanocylinders. *J. Am. Chem. Soc.* **2007**, *129* (17), 5630–5639.
- (45) Guérin, G.; Wang, H.; Manners, I.; Winnik, M. A. Fragmentation of Fiberlike Structures: Sonication Studies of Cylindrical Block Copolymer Micelles and Behavioral Comparisons to Biological Fibrils. *J. Am. Chem. Soc.* **2008**, *130* (44), 14763–14771.
- (46) Zhao, J.; Pispas, S.; Zhang, G. Effect of Sonication on Polymeric Aggregates Formed by Poly(Ethylene Oxide)-Based Amphiphilic Block Copolymers. *Macromol. Chem. Phys.* **2009**, *210* (12), 1026–1032
- (47) Huang, H.; Zhong, B.; Zu, X.; Luo, H.; Lin, W.; Zhang, M.; Zhong, Y.; Yi, G. Fabrication of Ordered Nanopattern by Using ABC Triblock Copolymer with Salt in Toluene. *Nanoscale Res. Lett.* **2017**, 12 (1), 491.
- (48) Ethirajan, A.; Punniyakoti, S.; D'Olieslaeger, M.; Wagner, P.; Boyen, H.-G. Ultrafast Self-Assembly Using Ultrasound: A Facile Route to the Rapid Fabrication of Well-Ordered Dense Arrays of

Inorganic Nanostructures. Angew. Chem., Int. Ed. 2013, 52 (37), 9709-9713.

- (49) Yokoyama, M.; Satoh, A.; Sakurai, Y.; Okano, T.; Matsumura, Y.; Kakizoe, T.; Kataoka, K. Incorporation of Water-Insoluble Anticancer Drug into Polymeric Micelles and Control of Their Particle Size. *J. Controlled Release* **1998**, *55*, 219–229.
- (50) Scheutjens, J. M. H. M.; Fleer, G. J. Statistical Theory of the Adsorption of Interacting Chain Molecules. 1. Partition Function, Segment Density Distribution, and Adsorption Isotherms. *J. Phys. Chem.* 1979, 83 (12), 1619–1635.
- (51) Matsuoka, T.; Masuda, Y.; Yamaguchi, T.; Koda, S. Observation of Ultrasonic Relaxation Due to Micelle-Monomer Exchange Process in Aqueous Solutions of Rodlike Micelles. *Jpn. J. Appl. Phys.* **2004**, 43 (5B), 2924–2925.
- (52) Ravichandran, G.; Gopinath, D. Ultrasonic Relaxation Studies on Micelle Formation in Aqueous Solutions of Some Bile Salts. *J. Mol. Liq.* **2014**, *198*, 122–127.
- (53) Lang, J.; Tondre, C.; Zana, R.; Bauer, R.; Hoffmann, H.; Ulbricht, W. Chemical Relaxation Studies of Micellar Equilibriums. *J. Phys. Chem.* **1975**, *79* (3), 276–283.
- (54) Gupta, S.; Bleuel, M.; Schneider, G. J. A New Ultrasonic Transducer Sample Cell for *in Situ* Small-Angle Scattering Experiments. *Rev. Sci. Instrum.* **2018**, 89 (1), 015111.
- (55) Hollamby, M. J. Practical Applications of Small-Angle Neutron Scattering. *Phys. Chem. Chem. Phys.* **2013**, *15* (26), 10566.
- (56) Hammouda, B. SANS from Polymers—Review of the Recent Literature. *Polym. Rev.* **2010**, *50* (1), 14–39.
- (57) Lund, R.; Willner, L.; Stellbrink, J.; Lindner, P.; Richter, D. Logarithmic Chain-Exchange Kinetics of Diblock Copolymer Micelles. *Phys. Rev. Lett.* **2006**, *96* (6), 068302.
- (58) Lund, R.; Willner, L.; Richter, D.; Dormidontova, E. E. Equilibrium Chain Exchange Kinetics of Diblock Copolymer Micelles: Tuning and Logarithmic Relaxation. *Macromolecules* **2006**, 39 (13), 4566–4575.
- (59) Lund, R.; Willner, L.; Richter, D.; Iatrou, H.; Hadjichristidis, N.; Lindner, P. Unraveling the Equilibrium Chain Exchange Kinetics of Polymeric Micelles Using Small-Angle Neutron Scattering Architectural and Topological Effects. *J. Appl. Crystallogr.* **2007**, *40* (s1), s327–s331.
- (60) Lund, R.; Willner, L.; Lindner, P.; Richter, D. Structural Properties of Weakly Segregated PS—PB Block Copolymer Micelles in *n* -Alkanes: Solvent Entropy Effects. *Macromolecules* **2009**, 42 (7), 2686—2695.
- (61) Choi, S.-H.; Bates, F. S.; Lodge, T. P. Molecular Exchange in Ordered Diblock Copolymer Micelles. *Macromolecules* **2011**, *44* (9), 3594–3604.
- (62) Kienzle, P. NCNR Neutron Activation and Scattering Calculator; https://www.ncnr.nist.gov/resources/activation/ (accessed Apr 24, 2018).
- (63) Wignall, G. D.; Littrell, K. C.; Heller, W. T.; Melnichenko, Y. B.; Bailey, K. M.; Lynn, G. W.; Myles, D. A.; Urban, V. S.; Buchanan, M. V.; Selby, D. L.; et al. The 40 m General Purpose Small-Angle Neutron Scattering Instrument at Oak Ridge National Laboratory. *J. Appl. Crystallogr.* **2012**, *45* (5), 990–998.
- (64) Zinn, T.; Willner, L.; Lund, R.; Pipich, V.; Richter, D. Equilibrium Exchange Kinetics in N-Alkyl—PEO Polymeric Micelles: Single Exponential Relaxation and Chain Length Dependence. *Soft Matter* **2012**, *8* (3), 623–626.
- (65) Iglesias, M.; Orge, B.; Tojo, J. Refractive Indices, Densities, and Excess Properties on Mixing of the Systems Acetone+ Methanol+ Water and Acetone+ Methanol+ 1-Butanol at 298.15 K. Fluid Phase Equilib. 1996, 126, 203–223.
- (66) González, B.; Calvar, N.; Gómez, E.; Domínguez, Á. Density, Dynamic Viscosity, and Derived Properties of Binary Mixtures of Methanol or Ethanol with Water, Ethyl Acetate, and Methyl Acetate at T = (293.15, 298.15, and 303.15) K. J. Chem. Thermodyn. 2007, 39, 1578–1588.
- (67) Brandrup, J.; Immergut, E. H.; Grulke, E. A.; Abe, A.; Bloch, D. R. *Polymer Handbook*, 4th ed.; John Wiley and Sons: New York, 1999.

(68) Lu, J.; Choi, S.; Bates, F. S.; Lodge, T. P. Molecular Exchange in Diblock Copolymer Micelles: Bimodal Distribution in Core-Block Molecular Weights. *ACS Macro Lett.* **2012**, *1* (8), 982–985.

- (69) Lu, J. Mechanisms of Chain Exchange in Block Copolymer Micelles, Ph.D. Dissertation, The University of Minnesota, 2015.
- (70) Duval, M.; Gross, E. Degradation of Poly(Ethylene Oxide) in Aqueous Solutions by Ultrasonic Waves. *Macromolecules* **2013**, *46* (12), 4972–4977.
- (71) Koda, S.; Taguchi, K.; Futamura, K. Effects of Frequency and a Radical Scavenger on Ultrasonic Degradation of Water-Soluble Polymers. *Ultrason. Sonochem.* **2011**, *18*, 276–281.
- (72) Antti, G.; Pentti, P.; Hanna, K. Ultrasonic Degradation of Aqueous Carboxymethylcellulose: Effect of Viscosity, Molecular Mass, and Concentration. *Ultrason. Sonochem.* **2008**, *15*, 644–648.
- (73) Koda, S.; Mori, H.; Matsumoto, K.; Nomura, H. Ultrasonic Degradation of Water-Soluble Polymers. *Polymer* **1994**, 35 (1), 30–33.
- (74) Yan, C.; Angus-Smyth, A.; Bain, C. D. Adsorption Kinetics of Non-Ionic Surfactants in Micellar Solutions: Effects of Added Charge. *Faraday Discuss.* **2013**, *160*, 45–61.
- (75) Schwenke, K.; Isa, L.; Del Gado, E. Assembly of Nanoparticles at Liquid Interfaces: Crowding and Ordering. *Langmuir* **2014**, *30* (11), 3069–3074.
- (76) Lee, J.; Ashokkumar, M.; Kentish, S.; Grieser, F. Determination of the Size Distribution of Sonoluminescence Bubbles in a Pulsed Acoustic Field. *J. Am. Chem. Soc.* **2005**, *127* (48), 16810–16811.
- (77) Segebarth, N.; Eulaerts, O.; Reisse, J.; Crum, L. A.; Matula, T. J. Correlation between Acoustic Cavitation Noise, Bubble Population, and Sonochemistry. *J. Phys. Chem. B* **2002**, *106* (35), 9181–9190.
- (78) Lee, J.; Kentish, S. E.; Ashokkumar, M. The Effect of Surface-Active Solutes on Bubble Coalescence in the Presence of Ultrasound. *J. Phys. Chem. B* **2005**, *109* (11), 5095–5099.
- (79) Tsochatzidis, N. A.; Guiraud, P.; Wilhelm, A. M.; Delmas, H. Determination of Velocity, Size and Concentration of Ultrasonic Cavitation Bubbles by the Phase-Doppler Technique. *Chem. Eng. Sci.* **2001**, *56*, 1831–1840.
- (80) Colegate, D. M.; Bain, C. D. Adsorption Kinetics in Micellar Solutions of Nonionic Surfactants. *Phys. Rev. Lett.* **2005**, *95*, 198302.
- (81) Bhole, N. S.; Huang, F.; Maldarelli, C. Fluorescence Visualization and Modeling of a Micelle-Free Zone Formed at the Interface between an Oil and an Aqueous Micellar Phase during Interfacial Surfactant Transport. *Langmuir* **2010**, *26* (20), 15761–15778
- (82) Ashokkumar, M. The Characterization of Acoustic Cavitation Bubbles An Overview. *Ultrason. Sonochem.* **2011**, *18*, 864–872.
- (83) Brotchie, A.; Grieser, F.; Ashokkumar, M. Effect of Power and Frequency on Bubble-Size Distributions in Acoustic Cavitation. *Phys. Rev. Lett.* **2009**, *102* (8), 084302.